www.sciencemag.org/cgi/content/full/321/5890/824/DC1

Supporting Online Material for

Programming DNA Tube Circumferences

Peng Yin,* Rizal F. Hariadi, Sudheer Sahu, Harry M.T. Choi, Sung Ha Park, Thomas H. LaBean, John H. Reif

*To whom correspondence should be addressed. E-mail: py@caltech.edu

Published 8 August 2008, *Science* **321**, 824 (2008)
DOI: 10.1126/science.1157312

This PDF file includes

Materials and Methods
SOM Text
Figs. S1 to S16
References

Supporting Online Material (SOM)

Programming DNA Tube Circumferences

Peng Yin[1,2,3†] Rizal F. Hariadi[4] Sudheer Sahu[6] Harry M.T. Choi[2]
Sung Ha Park[1,5*] Thomas H. LaBean[6,7] John H. Reif[6]

Department of Computer Science[1], Department of Bioengineering[2], Center for Biological Circuit Design[3],
Department of Applied Physics[4], Center for the Physics of Information[5],
Caltech, Pasadena, CA 91125, USA.
Department of Computer Science[6], Department of Chemistry[7], Duke University, Durham, NC 27708, USA.
* Present address: Department of Physics, SKKU Advanced Institute of Nanotechnology,
Sungkyunkwan University, Suwon, 440-746, Korea.
†To whom correspondence should be addressed. E-mail: py@caltech.edu

Materials and methods

DNA sequence design. DNA sequences for 3-, 4-, 5-, and 6-helix ribbon systems, and 4-, 5-, and 6-helix tube systems were designed and optimized using the SEQUIN software (*S1*) and the TileSoft software (*S2*) to minimize sequence symmetry (*S1*). The other systems were designed using an unpublished sequence design component of the NUPACK server (www.nupack.org) to maximize the affinity and specificity for the target structures (*S3*). Sometimes, manual optimization was further performed on selected regions.

Sample preparation. DNA strands were synthesized by Integrated DNA Technology, Inc. (www.idtdna.com) and purified by denaturing polyacrylamide gel electrophoresis or HPLC. The concentrations of the DNA strands were determined by the measurement of ultraviolet absorption at 260 nm. To assemble the structures, DNA strands were mixed stoichiometrically to a final concentration of $\sim$1 μM for 20-helix ribbons and 20-helix tubes and $\sim$3 μM for other structures in 1$\times$ TAE/Mg^{++} buffer (20 mM Tris, pH 7.6, 2 mM EDTA, 12.5 mM $MgCl_2$) and annealed in a water bath in a styrofoam box by cooling from 90°C to 23°C over a period of 24 to 72 hours.

AFM imaging. AFM images were obtained using an MultiMode SPM with a Nanoscope IIIa controller (Veeco, Santa Barbara, CA) equipped with an Analog Q-control to optimize the sensitivity of the tapping mode (nanoAnalytics GmbH, Münster, Germany). A $\sim$40 μL drop of 1$\times$ TAE/Mg^{++} followed by a $\sim$5 μL drop of annealed sample was applied onto the surface of a freshly cleaved mica and left for approximately 2 minutes. Sometimes, additional dilution of the sample was performed to achieve the desired sample density. On a few occasions, supplemental 1$\times$ TAE/8mM Ni^{++} was added to increase the strength of DNA-mica binding (*S4*). Before placing the fluid cell on top of the mica puck, an additional $\sim$20 μL of 1$\times$ TAE/Mg^{++} buffer was added to the cavity between the fluid cell and the AFM cantilever chip to avoid bubbles. The AFM tips used were either the short and thin cantilever in the DNP-S oxide sharpened silicon nitride cantilever chip (Veeco Probes, Camarillo, CA) or the short cantilever in the SiNi chip (BudgetSensors, Sofia, Bulgaria).

Fluorescence imaging and length measurements. For fluorescence microscopy imaging, the 5′-end of the U1 strand was labeled with a Cy3 fluorophore. A 4 μL drop of 10 nM SST sample was deposited onto an untreated coverslip. The light microscope is a home-built prism-based TIRF microscope. The samples were excited with 532 nm solid-state laser (CrystaLaser, Reno, NV). The Cy3 emission was detected by a 60$\times$, 1.2 NA water immersion objective (Nikon), a Dual-View 2-channel filter cube (Photometrics, Pleasanton, CA), and a C9100-02 electron multiplier CCD camera (Hamamatsu). The images were analyzed using the imageJ image processing software (NIH) and MATLAB. A threshold was applied to each image to differentiate the nanotubes and the glass surface. The "skeletonize" command in imageJ is used to reduce a tube image to a single pixel wide skeleton, and the length of the skeleton is measured to approximate the length of the tube.

Thermal transition profiles. Thermal transition experiments were performed using an AVIV 14DS spectrophotometer (AVIV Biomedical, Lakewood, NJ) equipped with a water bath temperature controller. UV absorbance at 260 nm was measured with a 1 nm bandwidth. The temperature step was set at 0.1°C with a 0.1°C dead-band and an equilibration time of 0.25 minute. Each data point was smoothed with its 10 nearest neighbors to reduce instrument noise.

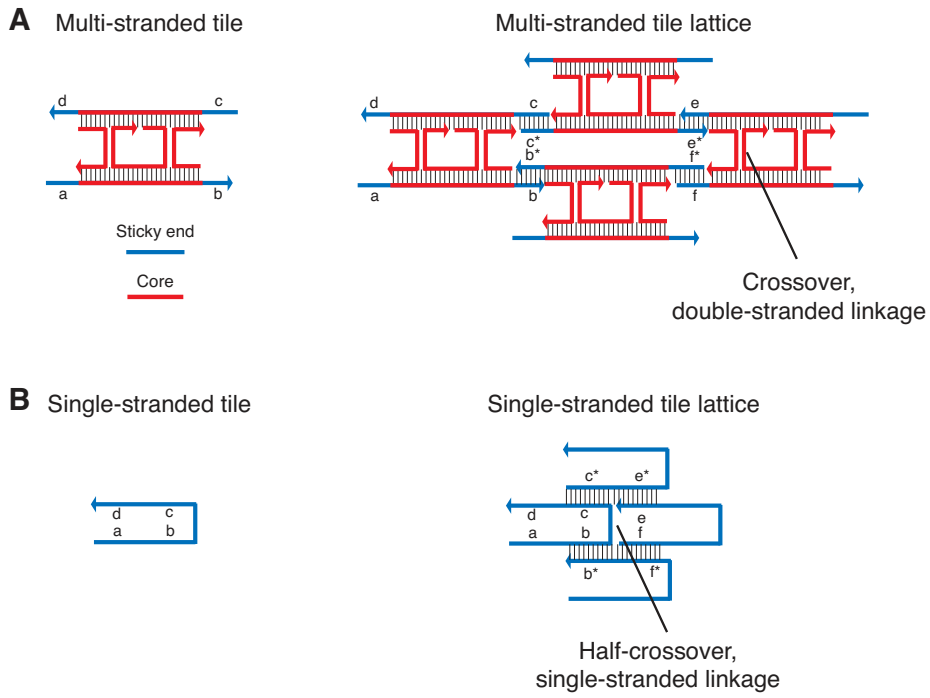

Fig. S1. Comparison between the multi-stranded tile and the single-stranded tile. (**A**) Left, a multi-stranded DX tile (*S5, S6*) contains a rigid structural core (red) and four flexible sticky ends (blue). Right, sticky end mediated self-assembly of DX tiles. The lattice structure comprises parallel DNA helices connected by double-stranded crossover points. Bold line segments represent the backbone of DNA; short black vertical bars represent base pairing; arrow heads indicate $3'$ ends. Letters marked with * are complementary to the corresponding unmarked letters. (**B**) Left, a single-stranded tile contains only sticky ends (i.e. domains). Right, sticky end mediated self-assembly of SST. The lattice structure comprises parallel DNA helices connected by half-crossover points (i.e. single-stranded linkage).

S1 Curvature analysis

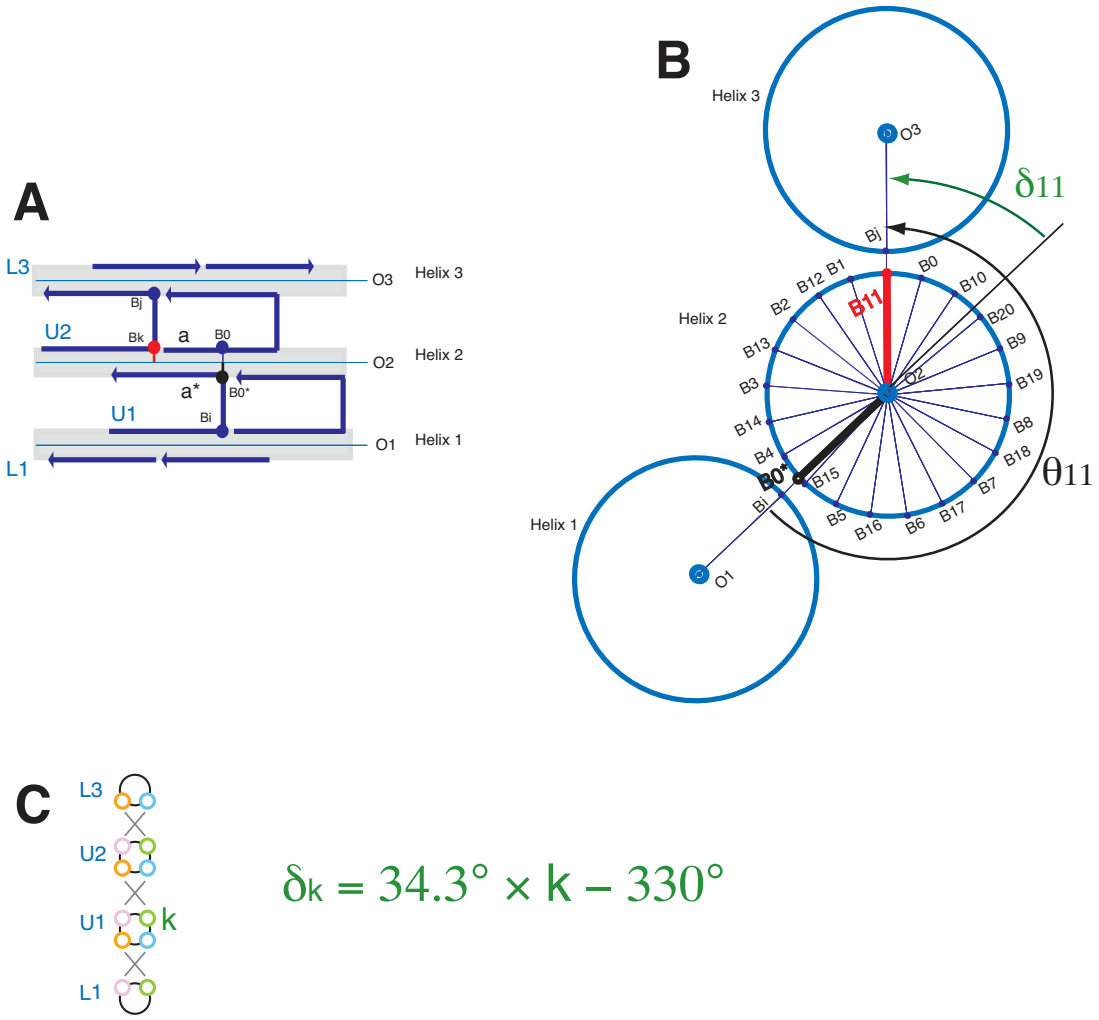

Fig. S2. Curvature analysis of unstrained SST lattices.

Adapting previously reported curvature analysis for DNA tubes (*S7, S8*), we describe below how to analyze the putative, approximate curvature of unstrained SST lattices (e.g. not closed into tubes).

We use a B-DNA model where 21 bases finish exactly two full helical turns. Now consider the three parallel helices depicted in fig. S2A. To study the curvature defined by the three axes O_1, O_2, and O_3, we depict the cross-section view in fig. S2B. In the cross section view, depict the projected positions of all the bases B_i in helix 2, where $i = 0, \ldots, 20$, on a circle. Note that B_i has exactly the same projected position as base $B_{i+21\times k}$, where k is a positive integer. Further depict the position of base B_{0^*}. Denote the counter clockwise angle from B_{0^*} to B_k as θ_k.

As 21 bases finish two full helical turns, the counterclockwise angle about the helix center between any two consecutive bases B_i and B_{i+1} is $\alpha = 360 \times 2/21 = 34.3°$. The counter clockwise angle from base B_0 to its complementary base B_{0^*} is $\beta = 150°$ (*S7*). Thus the counter clockwise angle from base B_{0^*} to base B_k is:

$$\theta_k = k \times \alpha - \beta = 34.3° \times k - 150°.$$

In fig. S2B, the angle $\theta_{11} = 227.3°$ is depicted.

In unstrained SST lattices, we assume that the two contacting helices H_i and H_{i+1} are approximately tangent to each other. Thus, in the cross-section view, the center O_i of helix H_i, the center O_{i+1} of helix H_{i+1}, and the two contacting bases that define the inter-helix linkage, all lie on the same line. In the case of fig. S2B, O_1, base B_i on Helix 1, base B_{0^*} on Helix 2, and O_2 lie

on the same line; O_2, base B_{11} on Helix 2, base B_j on Helix 3, and O_3 lie on the same line. We immediately have that the angle formed between the three helices O_1, O_2, and O_3 is θ_k. That is, the angle defined by O_1, O_2, and O_3 in fig. S2B is determined by the length k of domain a in fig. S2A. In the case of fig. S2, $k = 11$, and hence the angle is $\theta_{11} = 227.3°$. For ease of analysis, we further define a *curvature angle*

$$\delta_k = \theta_k - 180°.$$

Now consider the molecular program (fig. S2C) that defines the 3-helix ribbon lattice in fig. S2A. As the length of domain a in strand U2 in fig. S2A equals its complementary domain a^* in strand U1, which in turn equals the value k associated with the green port of U1 in fig. S2C, we immediately have the following formula for the curvature angle:

$$\delta_k = 34.3° \times k - 330°.$$

In fig. S2B, the angle $\delta_{11} = 47.3°$ is depicted.

Applying the above analysis, we immediately have that for the 3-, 4-, 5-, and 6-helix ribbons in Fig. 2 and the unclosed 4-, 5-, 6-, 7-, 8-, and 10-helix tubes in Fig. 4, which all have alternating 10-nt and 11-nt green ports, the curvature angles alternate between $\delta_{10} = 13°$ and $\delta_{11} = 47.3°$, averaging at $(\delta_{10}+\delta_{11})/2 = 30.2°$ per helix; and that for the 20-helix ribbon in Fig. 2 and the unclosed 20-helix tube in Fig. 4, which have only 10-nt green ports, the average curvature per helix is $\delta_{10} = 13°$.

Note that the above analysis is based on the assumption that in unstrained SST lattices, two adjacent helices lie approximately tangent to each other to minimize the putative molecular strain at the linkage points. This assumption, though theoretically plausible, has not been experimentally verified. Also note that the above analysis is intended for unstrained SST lattices and should not be applied to analyze the curvature of closed tubes.

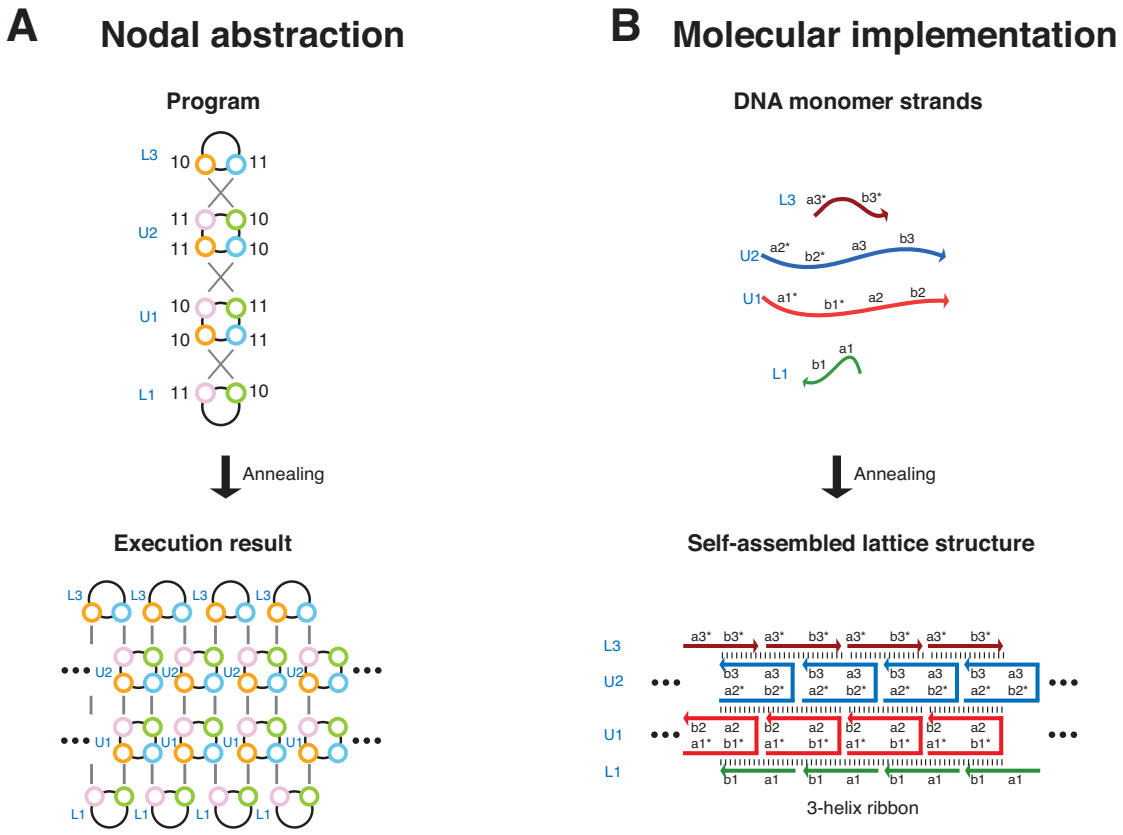

Fig. S3. Molecular program and secondary structure schematic for the 3-helix ribbon. (**A**) Top, the molecular program. The number associated with a port indicates the number of nucleotides in the corresponding domain in the SST motif. A gray line segment connects two complementary ports. Bottom, the lattice structure as the output of the program depicted in the top panel. (**B**) The molecular implementation of the program depicted in **A**. The domain dimensions correspond to the port dimensions depicted in **A**: L1, 10 (green port)-11 (pink port) (i.e. $|a_1|$ = 10 nt; $|b_1|$ = 11 nt); U1, 10-11-11-10; U2, 11-10-10-11; L3, 10-11. See SOM text S2 for DNA sequences.

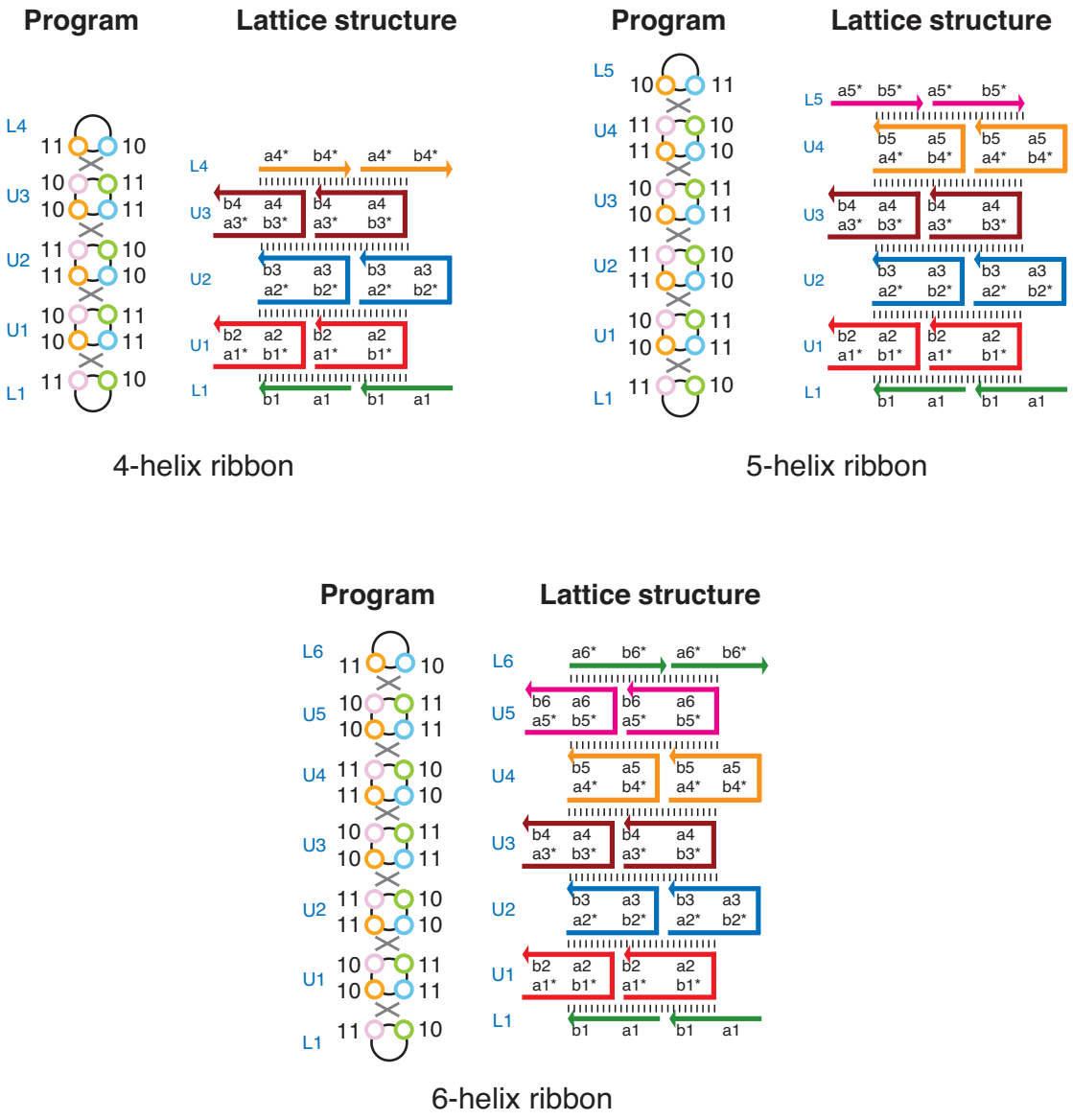

Fig. S4. Molecular programs and secondary structure schematics for 4-, 5-, and 6-helix ribbons. Left, molecular program. The number associated with a port indicates the number of nucleotides in the corresponding domain in the SST motif. A gray line segment connects two complementary ports. Right, secondary structure schematic. The domain dimensions correspond to the port dimensions depicted in the left panel: L1, 10-11; U1, U3, U5, 10-11-11-10; U2, U4, 11-10-10-11; L5, 10-11; L4, L6, 11-10. See SOM text S2 for DNA sequences.

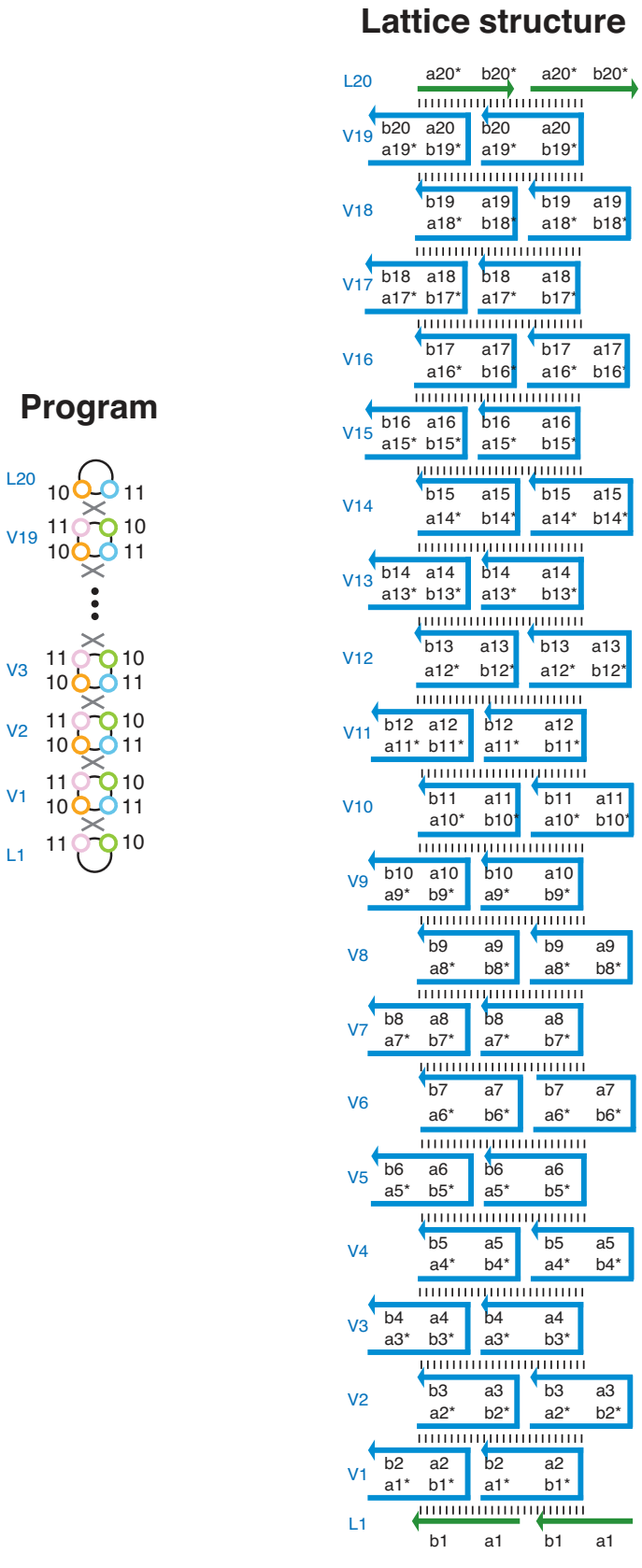

Fig. S4. Continued. Molecular program and secondary structure schematic for the 20-helix ribbon. The domain dimensions correspond to the port dimensions depicted in the left panel: L1, 10-11; V_k, 10-11-10-11; L20, 10-11. See SOM text S2 for DNA sequences.

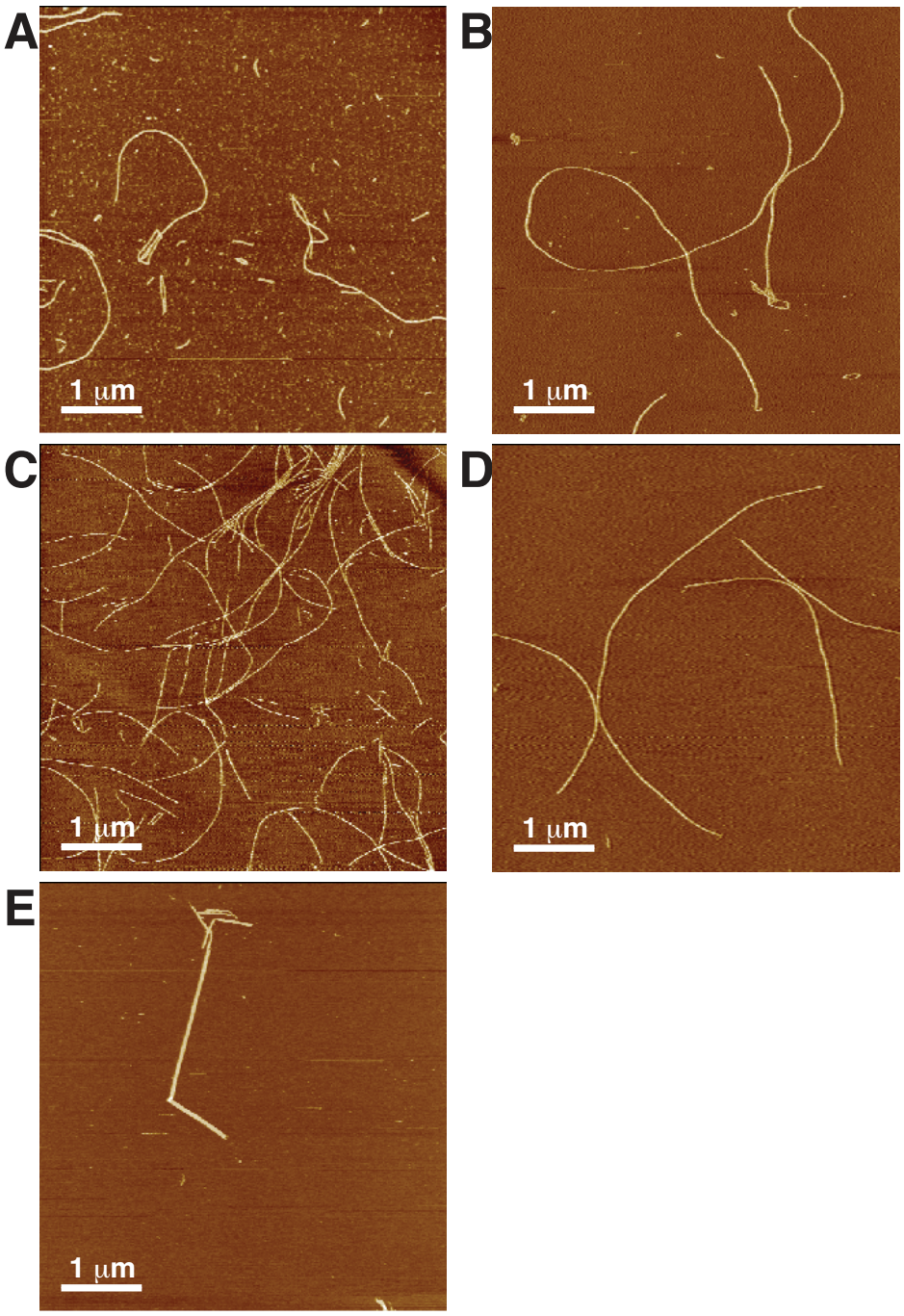

Fig. S5. AFM images of (**A**) 3-helix ribbons, (**B**) 4-helix ribbons, (**C**) 5-helix ribbons, (**D**) 6-helix ribbons, and (**E**) 20-helix ribbons. Some ribbons appear to "branch" in the AFM images. However, zoomed-in images reveal that such "branching" is primarily due to two ribbon segments lying (1) either on top of or (2) tangent to each other. It is likely that the first case results from two separate ribbon segments landing on the mica in a crossing configuration, and that the latter case occurs through electrostatic interactions between the ribbon segments during adsorption onto the mica surface. Though we cannot completely rule out the possibility that such two ribbon segments may share some edge strands, we suggest that such possibility is unlikely for the following reasons. First, in dilute samples, the crossing/tangent co-localization of the ribbons appears to be rare. Second, due to the flexibility of the single-stranded motif, an inter-ribbon linkage formed by one or two shared edge strands is likely to be unstable and may be dissolved respectively through three- or four-way branch migration.

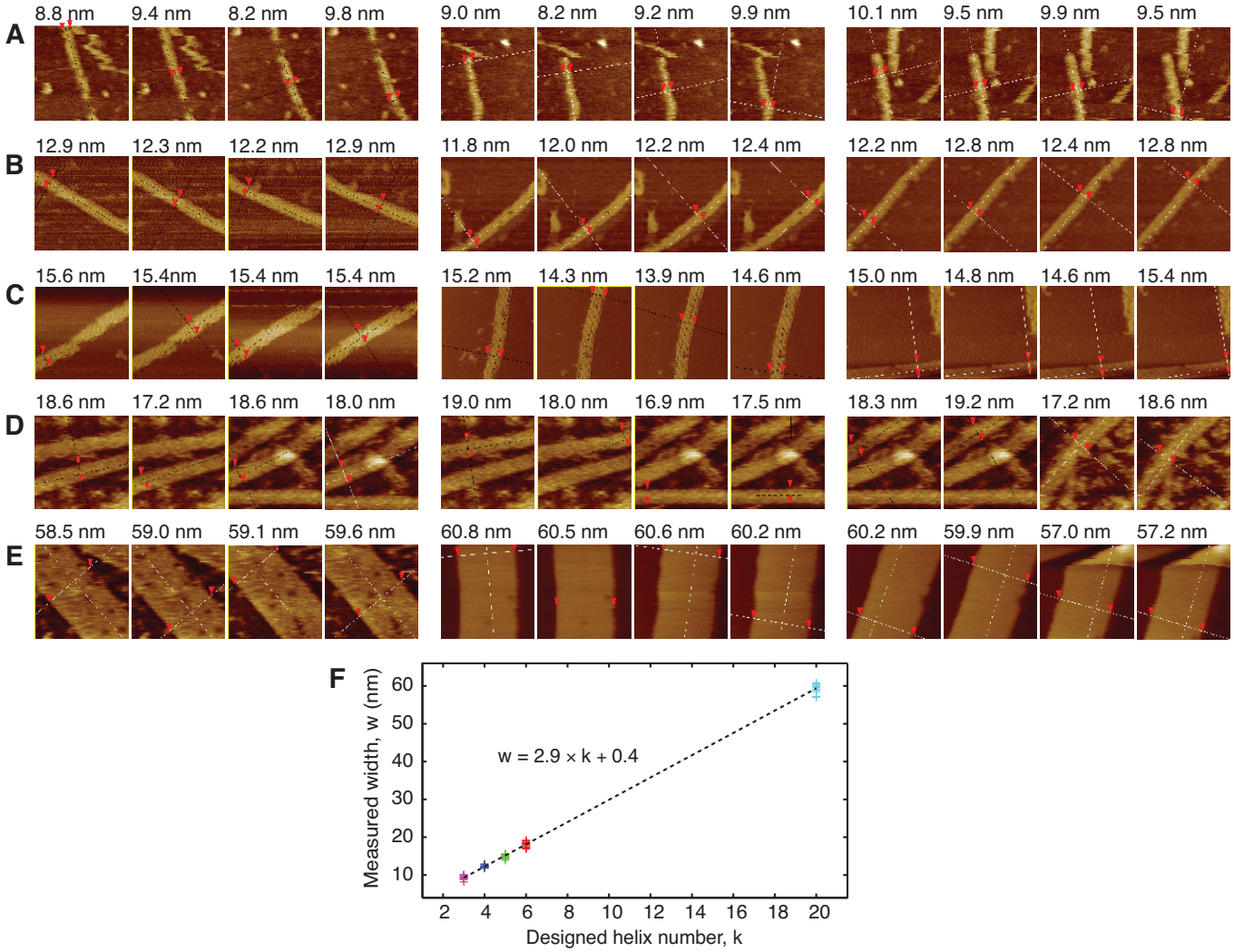

Fig. S6. SST ribbon width measurement. (**A-E**) 3-, 4-, 5-, 6-, and 20-helix ribbons. The section file screen shots are presented along with the measured widths of the ribbons. For each k-helix ribbon, three random samples were chosen; for each of these three samples, four random measurements were made. Image size: 100 nm $\times$ 100 nm. (**F**) Width plot. Linear fit reveals $w = 2.9 \times k + 0.4$, where w is the measured width and k is the designed helix number for the ribbon. This linear relationship is approximated by $w \approx 3 \times k$. This measured $\sim$3 nm per helix width for SST lattice is used in fig. S13 to establish the circumference monodispersity for k-helix tubes.

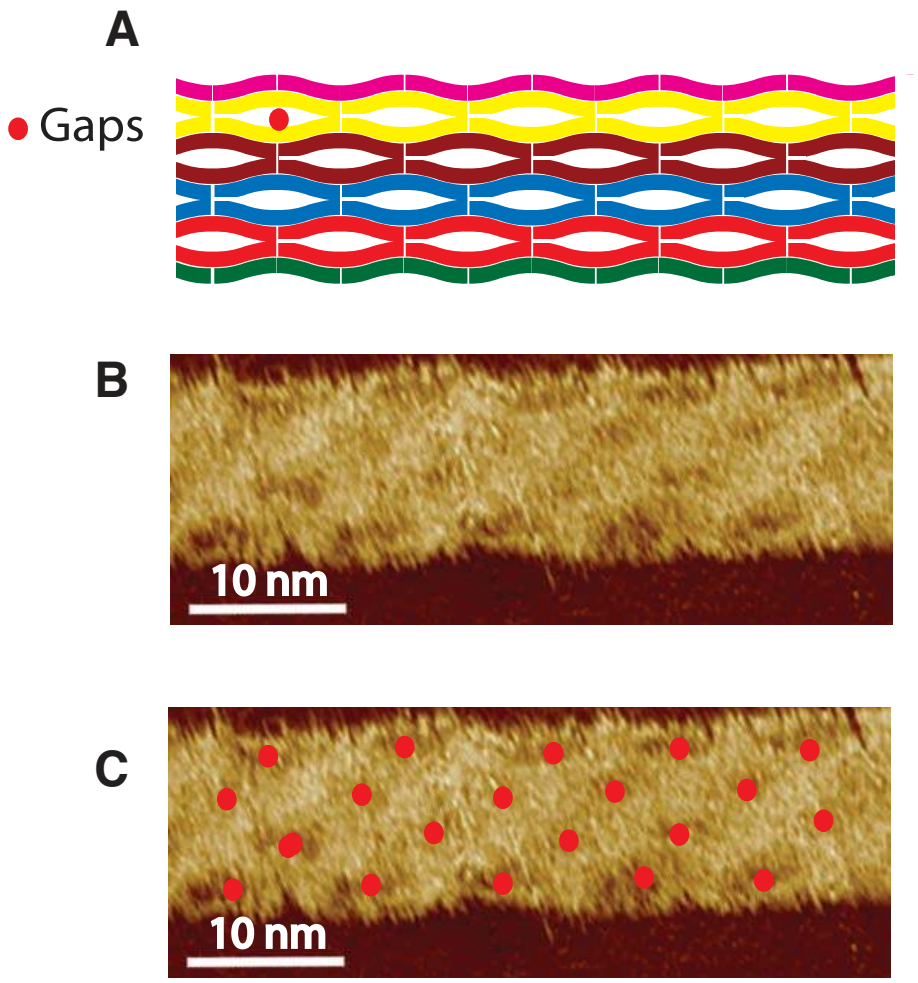

Fig. S7. High resolution AFM image for the 5-helix ribbon in Fig. 2C. (**A**) Schematic. (**B**) High resolution AFM image. (**C**) AFM image annotated with red dots indicating inter-helix gaps. The ∼3 nm per helix width measurement for k-helix ribbon structures is greater than the ∼2 nm width of a single DNA helix. The reason for this increased width is revealed in a high resolution image in fig. S7, which also presents further unambiguous evidence for the correct formation of the ribbon structures. (**A**) is a depiction of the expected DNA structure with bended helices and gaps between the helices. We suggest this structure may result from the following mechanism. The electrostatic force between neighboring negatively charged DNA helices pushes the helices away from each other, resulting in the bending of these helices, which are inter-connected by half-crossovers. The interplay between the electrostatic repulsion force and the bending deformation force is expected to result in a minimum energy lattice structure with alternating holes (indicated by red dots) and an increased width (*S9*). The AFM image of the 5-helix ribbon (**B**) agrees well with the above hypothesis, demonstrating an alternating pattern of four layers of inter-helix gaps (**C**).

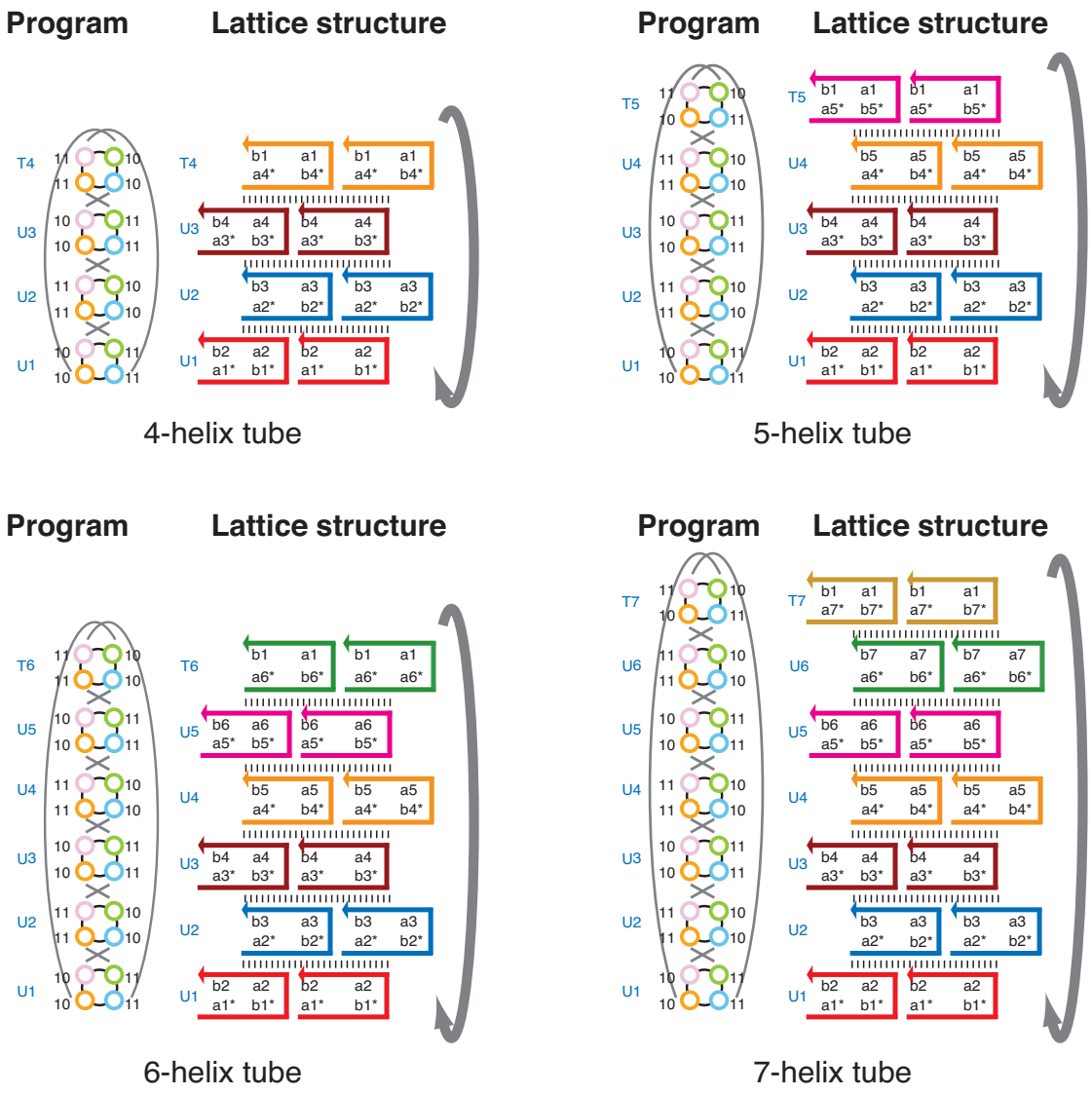

Fig. S8. The molecular programs and the secondary structures for 4-, 5-, 6-, 7-, 8-, and 10-helix tubes. Left, molecular program. The number associated with a port indicates the number of nucleotides in the corresponding domain in the SST motif. A gray line segment connects two complementary ports. Right, secondary structure schematic. The domain dimensions correspond to the port dimensions depicted in the left panel: U1, U3, U5, U7, and U9 have domain dimensions of 10-11-11-10; U2, U4, T4, U6, T6, U8, T8, and T10 have domain dimensions of 11-10-10-11; T5 and T7 have domain dimensions of 10-11-10-11. See SOM text S2 for DNA sequences.

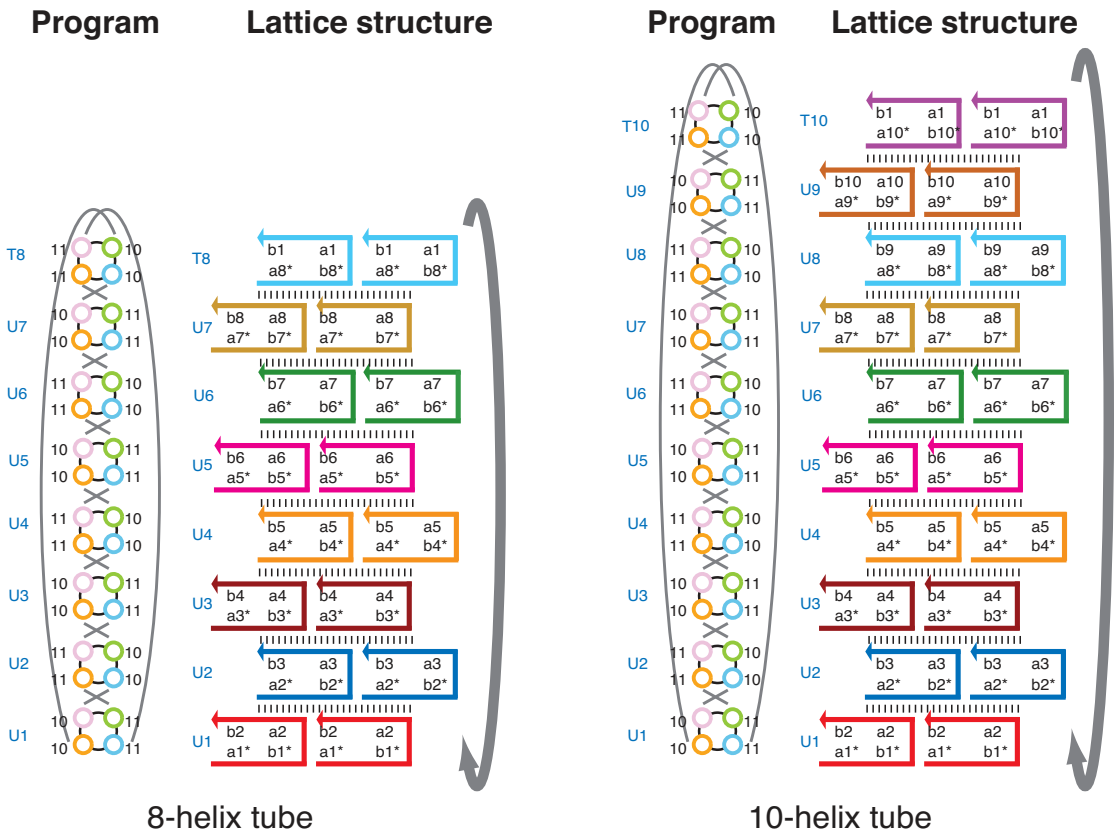

Fig. S8. Continued.

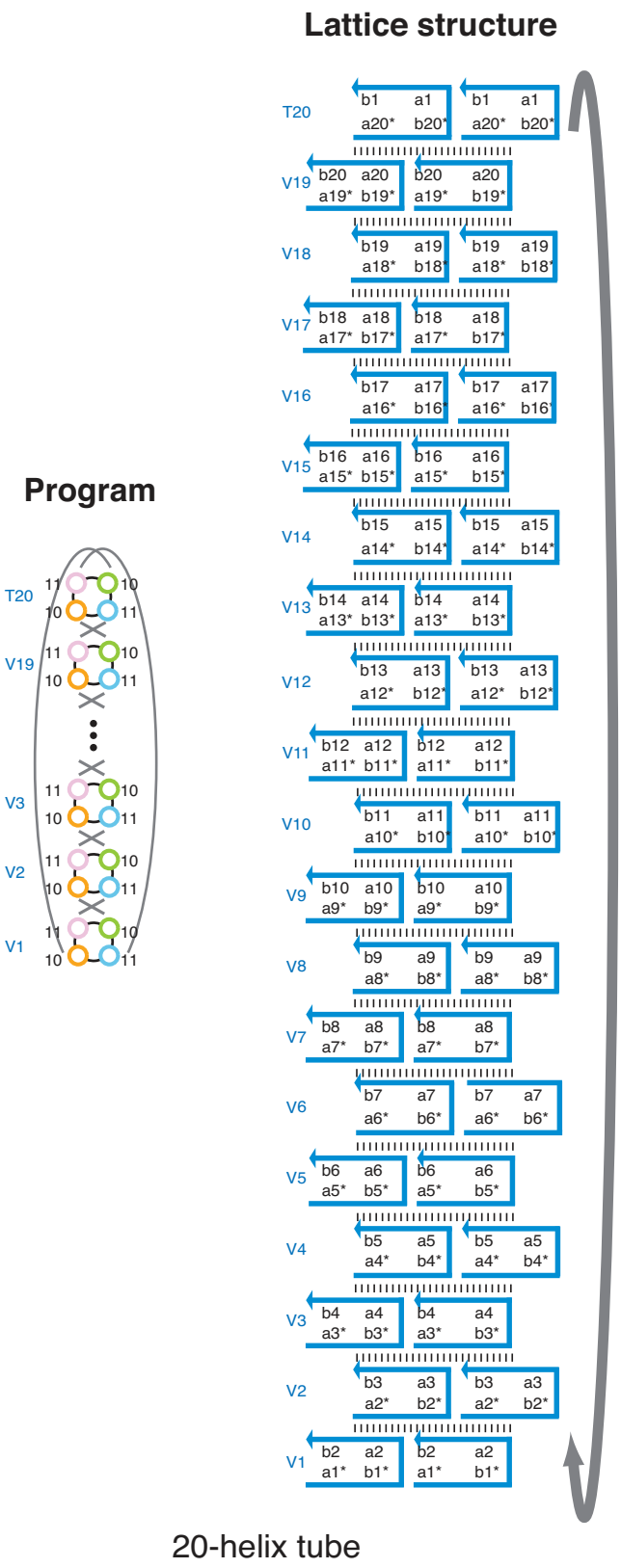

Fig. S8. Continued. Molecular program and the secondary structure for the 20-helix tube. The domain dimensions correspond to the port dimensions depicted in the left panel: V_k, T20, 10-11-10-11. See SOM text S2 for DNA sequences.

SST / Tubes	U1	U2	U3	U4	U5	U6	U7	U8	U9	T4	T5	T6	T7	T8	T10
4-helix tube	x	x	x							x					
5-helix tube	x	x	x	x							x				
6-helix tube	x	x	x	x	x							x			
7-helix tube	x	x	x	x	x	x							x		
8-helix tube	x	x	x	x	x	x	x							x	
10-helix tube	x	x	x	x	x	x	x	x	x						x

Fig. S9. The component strand table for 4-, 5-, 6-, 7-, 8-, and 10-helix tubes. The strands labeled with the same name are identical in fig. S8. Consequently, by selecting appropriate subsets from a common pool of 15 distinct 42-nt SST species (U1-9, T4-8, T10), we can construct monodisperse tubes with 6 distinct circumferences.

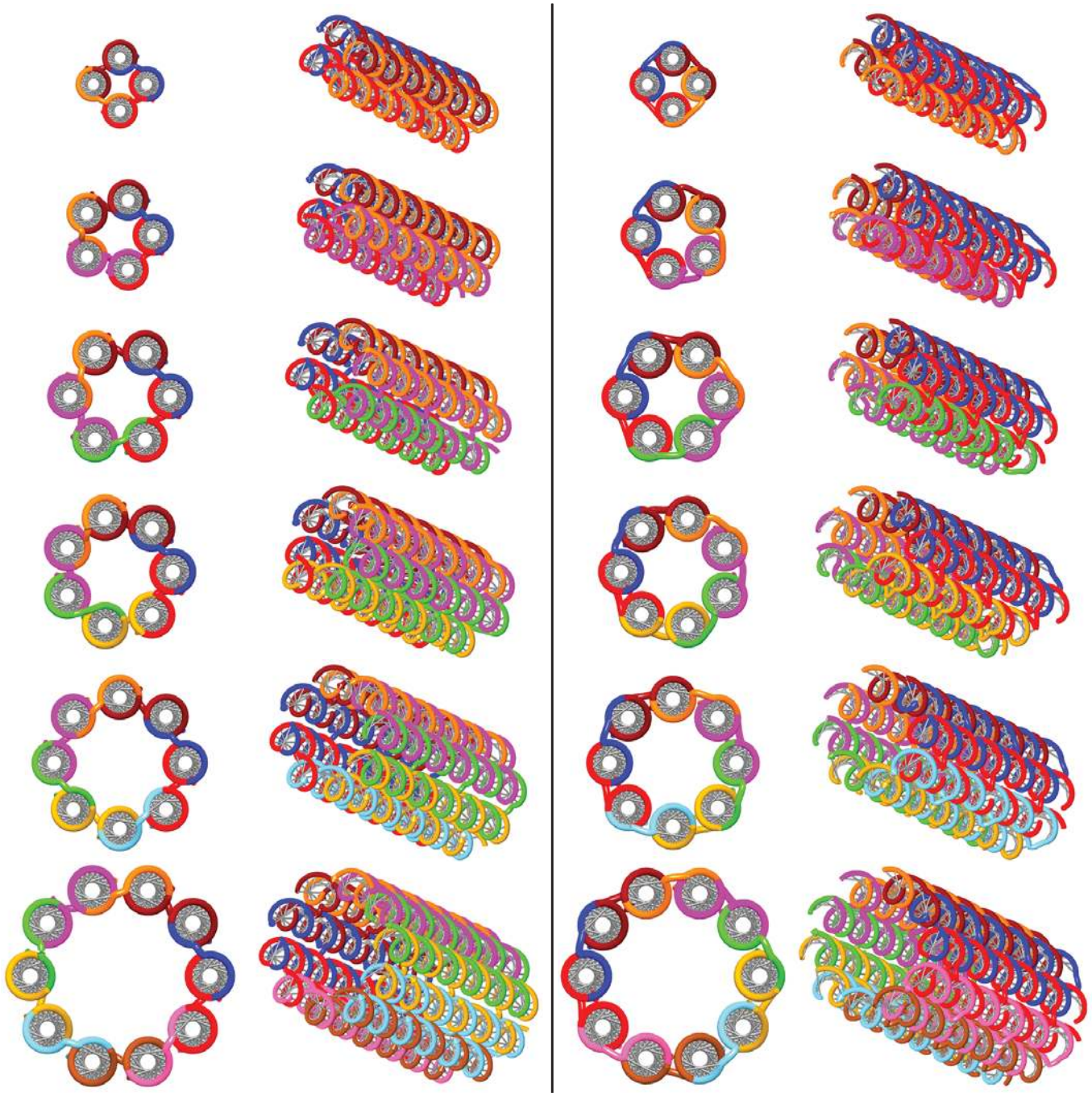

Fig. S10. 3D illustration of 4-, 5-, 6-, 7-, 8-, 10-, and 20-helix tubes. The figure shows both cross-section views and side views. The left column and the right column describe the tubes that are closed along opposite directions. In other words, a tube on the left is flipped inside out compared to the tube to its right. Based on this geometrical modeling, the configurations on the left appear to be less strained and are likely to dominate the configurations on the left thermodynamically. It is also conceivable the left configurations may dominate the right configurations kinetically, e.g. through faster cyclization. However, we have not performed experiments to characterize the closure directions of the SST tubes. It is also interesting to note the 10-base translational shift along the helix axial direction in the 5-helix tube and the 7-helix tube and the consequent putative mechanical strain that these tubes may have successfully absorbed.

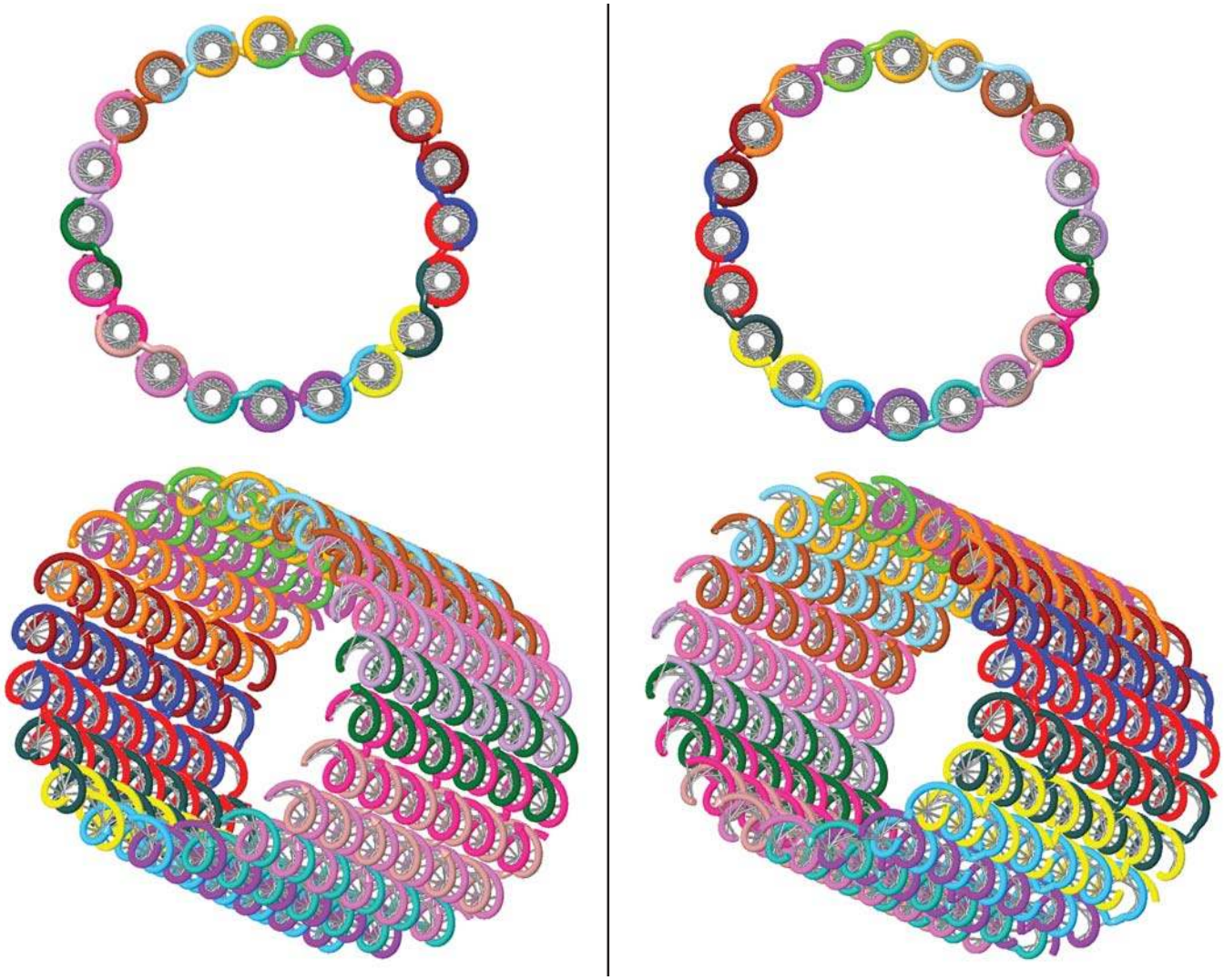

Fig. S10. Continued.

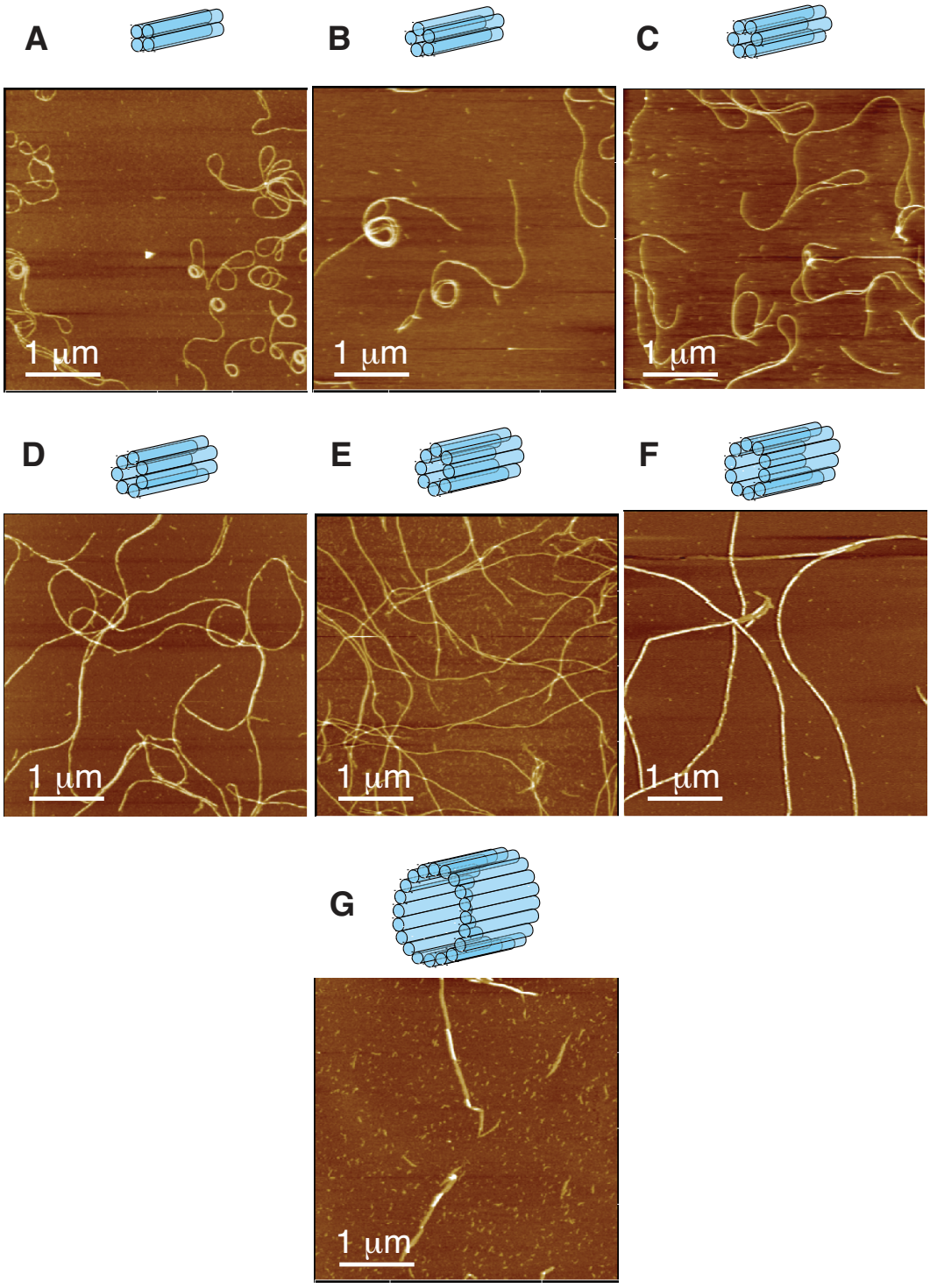

Fig. S11. Panels **A-G** are respectively AFM images of 4-, 5-, 6-, 7-, 8-, 10-, and 20-helix SST tubes. Note that the persistent lengths of the tubes appear to increase (as expected) with the number of the circumferential helices. Also note that the 4-helix tubes and 5-helix tubes sometimes appear in spiral configurations when deposited on mica. The presence of these spiral configurations may reflect the expected relatively shorter persistent lengths of the 4-helix and 5-helix tubes and/or the possibly relatively higher mechanical strain present in these tubes. Tube aggregations are commonly observed in 20-helix tubes and occasionally in other tube systems. Further, the 20-helix tubes typically appear significantly shorter than other tubes.

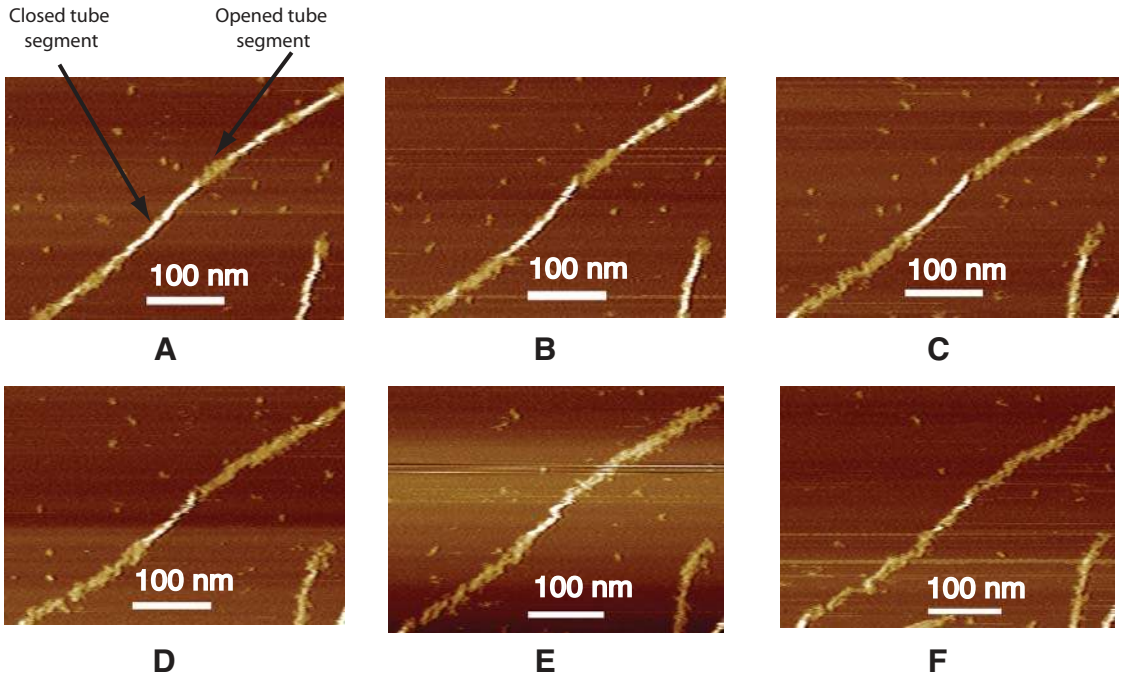

Fig. S12. AFM images for the opening of a 6-helix tube. The panels **A**-**F** present sequential screenshots demonstrating the process of the opening of a 6-helix tube by the repeated scanning of an AFM tip. The tube is opened by the mechanical force exerted by the AFM tip. The intact segments of the tube have higher height than the opened segments, and thus appear brighter. This process reveals the tubular nature of the 6-helix SST tubes.

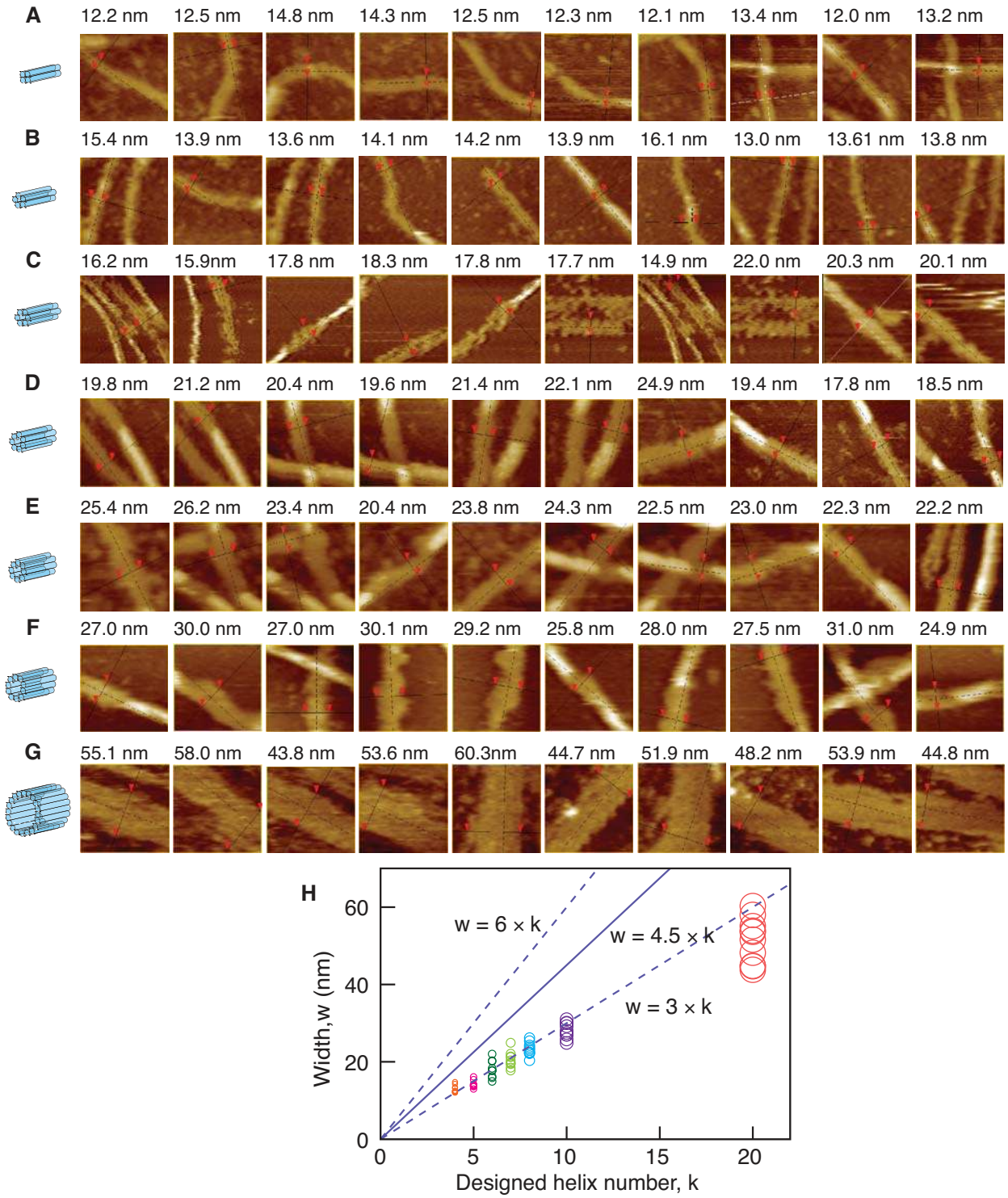

Fig. S13. SST tube circumference measurements. (**A-G**) 4-, 5-, 6-, 7-, 8-, 10-, and 20-helix tubes. The AFM section file screen shots are presented along with the measured widths of the opened tubes. Image size: 100 nm × 100 nm. (**H**) Width plot of opened tubes. A k-helix opened tube is expected to have a width $w \approx 3 \times k$ nm, as determined by the width measurement of the k-helix ribbons (fig. S6). A $2 \times k$-helix opened tube, by contrast, is expected have $w \approx 6 \times k$ nm. Lines corresponding to $w = 3 \times k$, $w = 4.5 \times k$, and $w = 6 \times k$ are plotted to facilitate tube circumference monodispersity determination. For each k-helix tube, 10 random, opened tubes are measured. Tube aggregations are commonly observed in 20-helix tubes and occasionally in other tube systems. Such aggregations are excluded from width measurements.

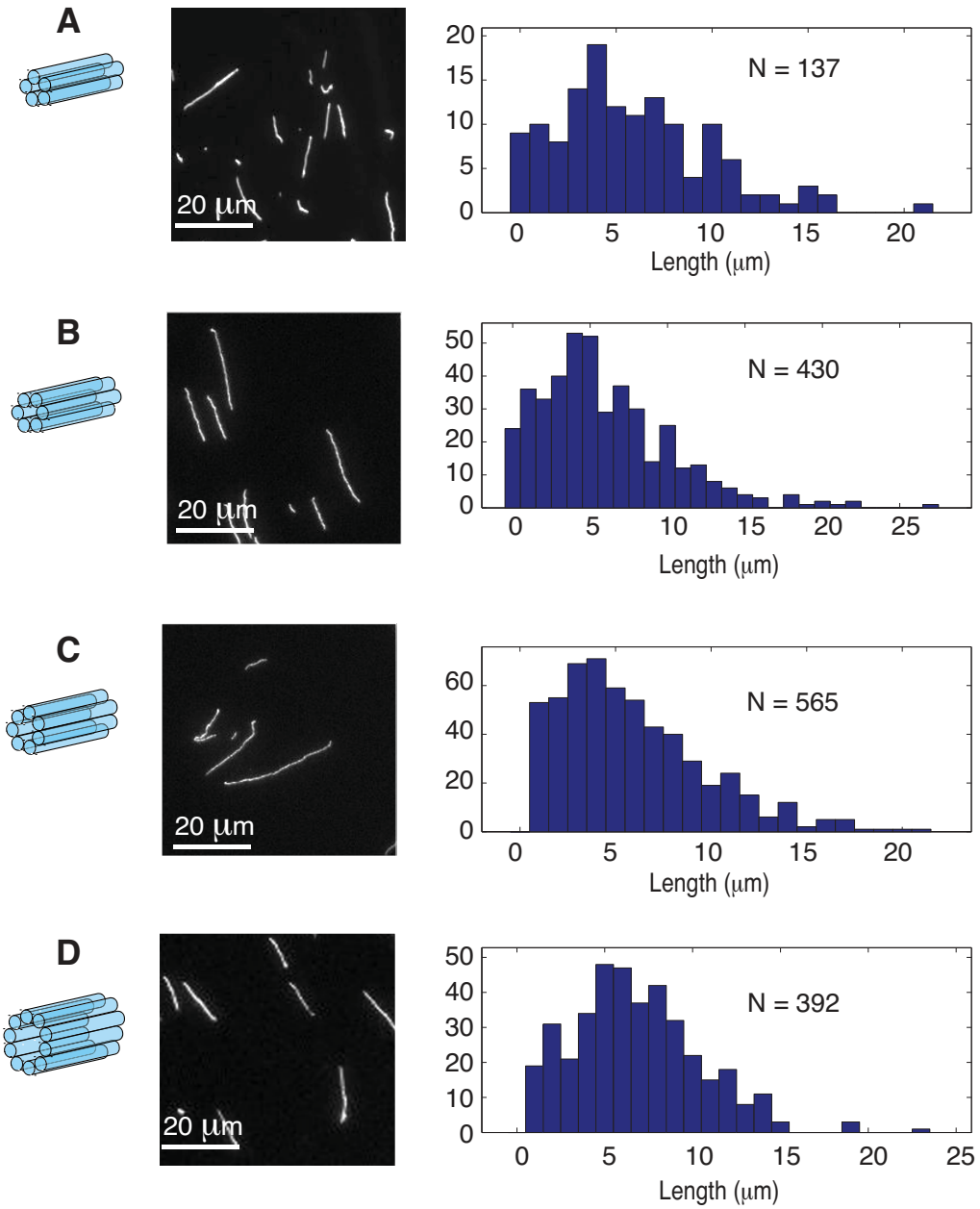

Fig. S14. Panels (**A-D**) are respectively fluorescence microscopy images (left) and length profile (right) of 5-, 6-, 7-, and 10-helix tubes decorated with Cy3 fluorophores. N denotes the sample size. The average lengths for 5-, 6-, 7-, and 10-helix tubes are respectively $\sim$5.9 μm, $\sim$5.9 μm, $\sim$5.8 μm, and $\sim$6.8 μm. To measure the lengths of the nanotubes, fluorescence microscopy is preferred over AFM for two reasons: (1) the fast exposure time of the light microscopy, which is on the order of 1 second per frame, as opposed to 200 seconds per frame for AFM; and (2) the larger view field.

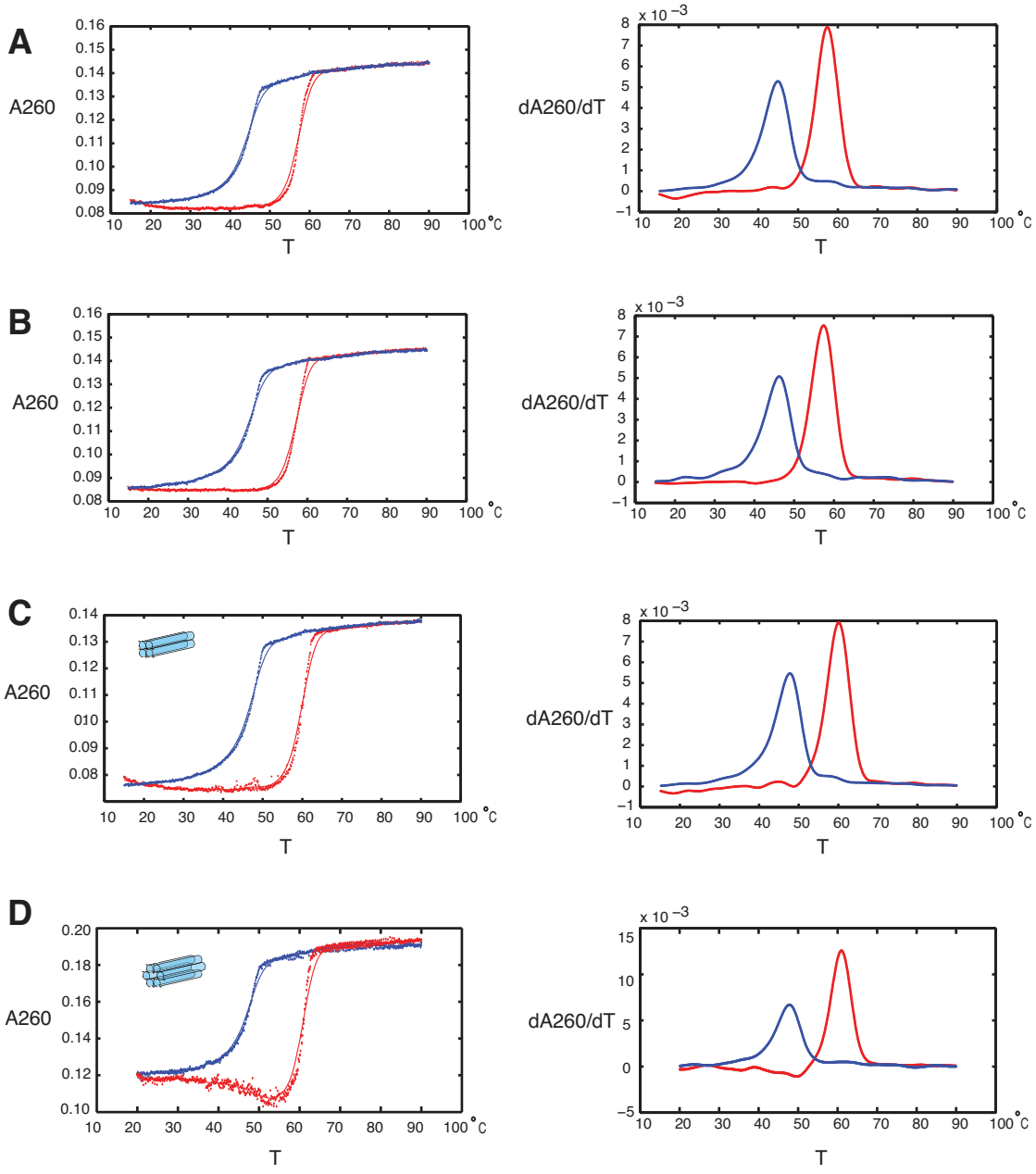

Fig. S15. Melting (red) and annealing (blue) curves for (**A**) 3-helix ribbons, (**B**) 4-helix ribbons, (**C**) 4-helix tubes, and (**D**) 6-helix tubes. The transition temperatures for melting/annealing (measured as the peaks of the derivates) are (A) 57°C and 45°C, (B) 58°C and 47°C, (C) 60°C and 48°C, and (D) 61°C and 48°C. Each constituent DNA strand at 100 nM. Cooling/heating rate at 0.15°C per minute for A-C and 0.115°C per minute for D. When repeating the experiment in D at a slower cooling/heating rate of 0.023°C per minute, the transition temperatures for melting/annealing become 60°C and 49°C (data not shown).

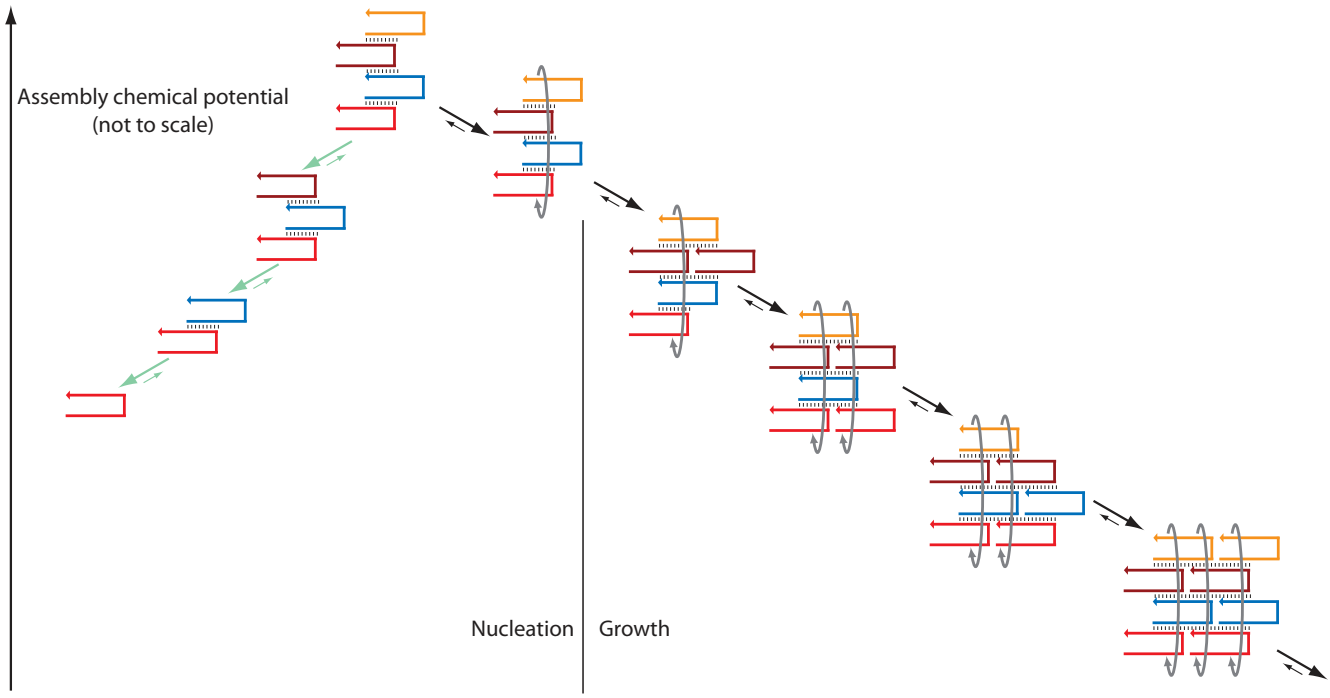

Fig. S16. Energetics of a conjectured assembly sequence for 4-helix SST tubes. To speculate about possible kinetic assembly pathways, we adapt a nucleation-elongation model in (*S10*). The figure describes a hypothetical pathway for assembling 4-helix SST tubes under slightly super saturated conditions, where the attachment of one SST to the lattice with two sticky ends (i.e. domains) is favorable but with one sticky end is unfavorable. The rate-limiting nucleation step (left) that involves unfavorable events leads to the formation of a presumed critical nucleus, followed by growth (right) composed of only favorable events. Note that the downhill growth steps involve the formation of approximately twice as many base pairs as the uphill nucleation steps. Large black arrows, forward-biased reaction steps. Small green arrows, unfavorable steps. The schematic is adapted from the depiction of the "standard sequence model" in (*S10*) .

S2 DNA sequences

The DNA sequences are presented as text sequences annotated with domain names. The domain names are consistent with those in the secondary structure schematics figures (figs. S3, S4, S8).

DNA sequences: 3-, 4-, 5-, 6-helix ribbons

```
U1: a1*-b1*-a2-b2
GGCGATTAGG-ACGCTAAGCCA-CCTTTAGATCC-TGTATCTGGT

U1-Cy3:
/5Cy3/TT-GGCGATTAGG-ACGCTAAGCCA-CCTTTAGATCC-TGTATCTGGT

U2: a2*-b2*-a3-b3
GGATCTAAAGG-ACCAGATACA-CCACTCTTCC-TGACATCTTGT

U3: a3*-b3*-a4-b4
GGAAGAGTGG-ACAAGATGTCA-CCGTGAGAACC-TGCAATGCGT

U4: a4*-b4*-a5-b5
GGTTCTCACGG-ACGCATTGCA-CCGCACGACC-TGTTCGACAGT

U5: a5*-b5*-a6-b6
GGTCGTGCGG-ACTGTCGAACA-CCAACGATGCC-TGATAGAAGT

L1: a1-b1
CCTAATCGCC-TGGCTTAGCGT

L3: a3*-b3*
GGAAGAGTGG-ACAAGATGTCA

L4: a4*-b4*
GGTTCTCACGG-ACGCATTGCA

L5: a5*-b5*
GGTCGTGCGG-ACTGTCGAACA

L6: a6*-b6*
GGCATCGTTGG-ACTTCTATCA
```

DNA sequences: 20-helix ribbons

Note that strands V1 and U1 have identical sequences, but different domain partitions. The same is true for V3 and U3, and V5 and U5. L1 is the same as in the previous section.

```
V1: a1*-b1*-a2-b2
GGCGATTAGG-ACGCTAAGCCA-CCTTTAGATC-CTGTATCTGGT

V2: a2*-b2*-a3-b3
GATCTAAAGG-ACCAGATACAG-CCACTCTTCC-TGACATCTTGT

V3: a3*-b3*-a4-b4
GGAAGAGTGG-ACAAGATGTCA-CCGTGAGAAC-CTGCAATGCGT

V4: a4*-b4*-a5-b5
GTTCTCACGG-ACGCATTGCAG-CCGCACGACC-TGTTCGACAGT

V5: a5*-b5*-a6-b6
GGTCGTGCGG-ACTGTCGAACA-CCAACGATGC-CTGATAGAAGT

V6: a6*-b6*-a7-b7
GCATCGTTGG-ACTTCTATCAG-ATGCACCTCC-AGCTTTGAATG

V7: a7*-b7*-a8-b8
GGAGGTGCAT-CATTCAAAGCT-AACGGTAACT-ATGACTTGGGA
```

```
V8: a8*-b8*-a9-b9
AGTTACCGTT-TCCCAAGTCAT-AACACTAGAC-ACATGCTCCTA

V9: a9*-b9*-a10-b10
GTCTAGTGTT-TAGGAGCATGT-CGAGACTACA-CCCTTGCCACC

V10: a10*-b10*-a11-b11
TGTAGTCTCG-GGTGGCAAGGG-TACTACCGCT-CCATTAAGAAT

V11: a11*-b11*-a12-b12
AGCGGTAGTA-ATTCTTAATGG-ATCCGTCTAT-CTACACTATCA

V12: a12*-b12*-a13-b13
ATAGACGGAT-TGATAGTGTAG-AGACGAAATC-AGCAGAACTAA

V13: a13*-b13*-a14-b14
GATTTCGTCT-TTAGTTCTGCT-CTGCGAAGTA-ATCAGCCGAGC

V14: a14*-b14*-a15-b15
TACTTCGCAG-GCTCGGCTGAT-GAACTCGCTC-CAGAATCGACG

V15: a15*-b15*-a16-b16
GAGCGAGTTC-CGTCGATTCTG-AACTTTCAAT-ATCATATCGTA

V16: a16*-b16*-a17-b17
ATTGAAAGTT-TACGATATGAT-CCGTAGCAGT-ATAAGCGATCT

V17: a17*-b17*-a18-b18
ACTGCTACGG-AGATCGCTTAT-CGCTAGCCAC-CAAGATCAAGC

V18: a18*-b18*-a19-b19
GTGGCTAGCG-GCTTGATCTTG-CAATCGGACC-TGCCTTATCCT

V19: a19*-b19*-a20-b20
GGTCCGATTG-AGGATAAGGCA-GACACGGCAC-CACTTACTCAT

L20: a20*-b20*
GTGCCGTGTC-ATGAGTAAGTG
```

DNA sequences: 4-, 5-, 6-, 7-, 8-, 10-helix tubes

The sequences for strands U1 to U6 are listed above. Note that strand U7 and V7 have identical sequences, but different domain partitions. The same is true for U9 and V9, and U11 and V11.

```
U6: a6*-b6*-a7-b7
GGCATCGTTGG-ACTTCTATCA-ATGCACCTCC-AGCTTTGAATG

U7: a7*-b7*-a8-b8
GGAGGTGCAT-CATTCAAAGCT-AACGGTAACTA-TGACTTGGGA

U8: a8*-b8*-a9-b9
TAGTTACCGTT-TCCCAAGTCA-AACACTAGAC-ACATGCTCCTA

U9: a9*-b9*-a10-b10
GTCTAGTGTT-TAGGAGCATGT-CGAGACTACAC-CCTTGCCACC

T4: a4*-b4*-a1-b1
GGTTCTCACGG-ACGCATTGCA-CCTAATCGCC-TGGCTTAGCGT

T5: a5*-b5*-a1-b1
GGTCGTGCGG-ACTGTCGAACA-CCTAATCGCC-TGGCTTAGCGT

T6: a6*-b6*-a1-b1
GGCATCGTTGG-ACTTCTATCA-CCTAATCGCC-TGGCTTAGCGT

T7: a7*-b7*-a1-b1
GGAGGTGCAT-CATTCAAAGCT-CCTAATCGCC-TGGCTTAGCGT

T8: a8*-b8*-a1-b1
TAGTTACCGTT-TCCCAAGTCA-CCTAATCGCC-TGGCTTAGCGT
```

```
T10: a10*-b10*-a1-b1
GTGTAGTCTCG-GGTGGCAAGG-CCTAATCGCC-TGGCTTAGCGT
```

DNA sequences: 20-helix tubes

The sequences for strands V1 to V19 are listed above.

```
T20: a20*-b20*-a1-b1
GTGCCGTGTC-ATGAGTAAGTG-CCTAATCGCC-TGGCTTAGCGT
```

References and Notes

[S1] N. C. Seeman, *J. Biomol. Struct. Dyn.* **8**, 573 (1990).
[S2] P. Yin, *et al.*, TileSoft: Sequence optimization software for designing DNA secondary structures, *Tech. Rep. CS-2004-09*, Duke University, Computer Science Department (2004).
[S3] R. M. Dirks, M. Lin, E. Winfree, N. A. Pierce, *Nucleic Acids Res.* **32**, 1392 (2004).
[S4] H. G. Hansma, D. E. Laney, *Biophys. J.* **70**, 1933 (1996).
[S5] T. J. Fu, N. C. Seeman, *Biochemistry* **32**, 3211 (1993).
[S6] E. Winfree, F. Liu, L. A. Wenzler, N. C. Seeman, *Nature* **394**, 539 (1998).
[S7] P. W. K. Rothemund, *et al.*, *J. Am. Chem. Soc.* **126**, 16344 (2004).
[S8] W. B. Sherman, N. C. Seeman, *Biophys. J.* **90**, 4546 (2006).
[S9] R. Hariadi, E. Winfree, *Foundations of Nanoscience (Poster)* (2004), vol. 1.
[S10] R. Schulman, E. Winfree, *Proc. Natl. Acad. Sci. USA* **104**, 15236 (2007).